Letter

Electric-field-induced crossover of polarization reversal mechanisms in Al$_{1-x}$Sc$_x$N ferroelectrics

Aravind Krishnamoorthy[1] , Subodh C Tiwari[1], Aiichiro Nakano,
Rajiv K Kalia and Priya Vashishta

Collaboratory for Advanced Computing and Simulations, University of Southern California, Los Angeles,
CA 90089-0242, United States of America

E-mail: priyav@usc.edu

CrossMark

Abstract
Scandium-doped aluminum nitride, Al$_{1-x}$Sc$_x$N, represents a new class of displacive ferroelectric materials with high polarization and sharp hysteresis along with high-temperature resilience, facile synthesizability and compatibility with standard CMOS fabrication techniques. The fundamental physics behind the transformation of unswitchable piezoelectric AlN into switchable Al–Sc–N ferroelectrics depends upon important atomic properties such as local structure, dopant distributions and the presence of competing mechanism of polarization switching in the presence of an applied electric-field that have not been understood. We computationally synthesize Al$_{1-x}$Sc$_x$N to quantify the inhomogeneity of Sc distribution and phase segregation, and characterize its crystal and electronic structure as a function of Sc-doping. Nudged elastic band calculations of the potential energy surface and quantum molecular dynamics simulations of direct electric-field-driven ferroelectric switching reveal a crossover between two polarization reversal mechanisms—inhomogeneous nucleation-and-growth mechanism originating near Sc-rich regions in the limit of low applied fields and nucleation-limited-switching in the high-field regime. Understanding polarization reversal pathways for these two mechanisms as well as the role of local Sc concentration on activation barriers provides design rules to identify other combinations of dopant elements, such as Zr, Mg etc. to synthesize superior AlN-based ferroelectric materials.

Supplementary material for this article is available online

Keywords: ferroelectric, aluminum nitride, polarization switching, scandium

(Some figures may appear in colour only in the online journal)

1. Introduction

Ferroelectric switching is a reversible electric-field-induced transition between two equivalent states of spontaneous polarization not accompanied by significant diffusion, mass transport, or heat exchange [1]. Devices based on ferroelectrics leverage the switching of spontaneous electric polarization from one stable minimum to another in the presence of coercive electric-field. Understanding deterministic polarization reversal in ferroelectric materials is critical for their exploitation in nanoelectronic device applications [2], including ferroelectric domain wall 'racetrack' memory and photoelectric logic elements [3–5], nonvolatile random access memories [6], ferroelectric tunnel junctions, [7] and high-density data storage [8] and neural computing [9].

[1] Authors contributed equally.

Traditional ferroelectric materials like perovskites have several shortcomings including low paraelectric transition temperatures, long and diffusive transition in hysteresis curve between two polarization states as well as limited compatibility with complementary metal-oxide-semiconductor or III-nitride technology, which have hindered the application of ferroelectric functionality in nanoelectronics [10, 11]. Therefore, there is considerable scientific interest in novel ferroelectric materials such as orthorhombic HfO_2 [12–14] and nitrides [15–17] for next-generation logic and memory and neuromorphic devices [18], in addition to more traditional applications in sensors and microelectromechanical actuators [19, 20].

Akiyama *et al* demonstrated that the piezoresponse of solid solutions of high-temperature piezoelectric AlN [21] and nonpolar ScN [22] increases monotonously with Sc content [23, 24]. Fichtner *et al* confirmed the presence of ferroelectricity in the resulting $Al_{1-x}Sc_xN$ solid solution [25]. This unexpected discovery is highly significant because $Al_{1-x}Sc_xN$ ferroelectrics overcome many technological challenges through a combination of large spontaneous polarization (60–100 $\mu C\,cm^{-2}$), tunable coercive voltage (1.8–4.0 $MV\,cm^{-1}$), and low fabrication temperature (300 K) and compatibility with existing III-nitride synthesis technology, which together, makes Al–Sc–N ferroelectrics highly attractive for microelectronic device applications [26].

The atomic mechanism of polarization reversal including details about switching pathways and intermediate atomic configurations as well as the impact of Sc concentration and segregation are undetermined. Transmission electron microscopy studies of ferroelectric switching in bulk crystals aimed at characterizing atomistic mechanisms of the switching process have been limited due to difficulties in capturing the ultrafast switching process [27–30]. Therefore, atomistic modeling an ideal tool to investigate these microscopic properties. Specifically, density functional theory (DFT)-based quantum molecular dynamics (QMD) can provide atomistic information about the polarization reversal process in these ferroelectrics. Of particular interest is the question of whether phase transitions in this system is homogeneous, as suggested by the sharp hysteresis curve, or mediated by nucleation and growth of reverse-polarized domains [31]. It is also important to understand if the identified mechanism is different in strongly driven (i.e. intense applied fields) or ultrafast switching conditions, as hypothesized by recent semi-empirical phase field modeling studies.

In this article, we address both questions by investigating pathways and kinetics of field-driven polarization switching in a range of $Al_{1-x}Sc_xN$ alloys ($x = 0.0$–0.5) to systematically understand the role of material composition, Sc distribution and applied field on the polarization reversal mechanism. Simulations show a conventional nucleation and domain growth mechanism in the limit of low applied fields, with nucleation initiated at sites with larger local concentration of Sc ions and proceeding through the low-energy transition state involving 5-coordinated Sc ions. On the other hand, during strongly driven ferroelectric switching, polarization reversal occurs via a nucleation-limited-switching mechanism with independent nucleation events. Local inhomogeneities in Sc concentration can greatly affect both the onset and extent of ferroelectric switching in both mechanisms.

The next section describes the methods used to perform computational synthesis of the $Al_{1-x}Sc_xN$ system, as well as methods to perform *ab initio* simulations to understand polarization switching mechanisms and QMD simulations for direct field-driven polarization reversal. We then discuss our results on the phase stability of $Al_{1-x}Sc_xN$ structures, the potential energy surface (PES) during the switching process and dynamics of field-driven switching and conclude with a discussion of the role of local distribution of Sc dopants on the energetics and dynamics of the switching process.

2. Methods

The local structure around Al, Sc and N ions in $Al_{1-x}Sc_xN$ alloys is generated using *ab initio* MD simulations by slowly annealing a high-temperature (4500 K) Al–Sc–N melt down to room temperature over 6 ps. This rapid annealing rate is an artifact of the extremely short trajectory timescales accessible in QMD. However, quantitative metrics about local structure including bond-length and bond-angle distributions from the 6 ps annealing schedule were found to be identical to structures generated through a significantly longer 20 ps annealing schedule from the same temperature (figure S1 (available online at stacks.iop.org/NANO/32/49LT02/mmedia)) and are consistent with prior analyses of the effect of annealing rates on generated structures in aluminum ceramics [32]. This slow annealing ensures that structural metrics like local coordination and crystal structure are consistent with sputter-deposited experimental samples synthesized in prior experimental studies. The same procedure is repeated for multiple $Al_{1-x}Sc_xN$ compositions ($0 < x < 0.5$) to understand structure as a function of Sc content. We study the PES during polarization switching using nudged elastic band (NEB) simulations on wurtzite AlN crystals substitutionally doped with different concentrations of Sc. To study the switching of spontaneous polarization, we perform QMDs simulation at 300 K in the presence of electric fields ranging from 15 to 40 $MV\,cm^{-1}$. Electric-field application in molecular dynamics follows the formulation of Umari *et al* [33]. Further details on QMDs simulation are given in supplementary materials.

3. Results

3.1. Structure and electromechanical properties of $Al_{1-x}Sc_xN$ crystals

Figure 1 shows the computed per-formula-unit energies and relative stabilities of $Al_{1-x}Sc_xN$ in the wurtzite and rocksalt crystal structures. The phase boundary, determined as the crossover point in the per-formula-unit energies of the wurtzite and rocksalt structures, lies at 28%–43% Sc concentration, not accounting for finite-temperature effects. $Al_{1-x}Sc_xN$ adopts the wurtzite structure of AlN with substitutional
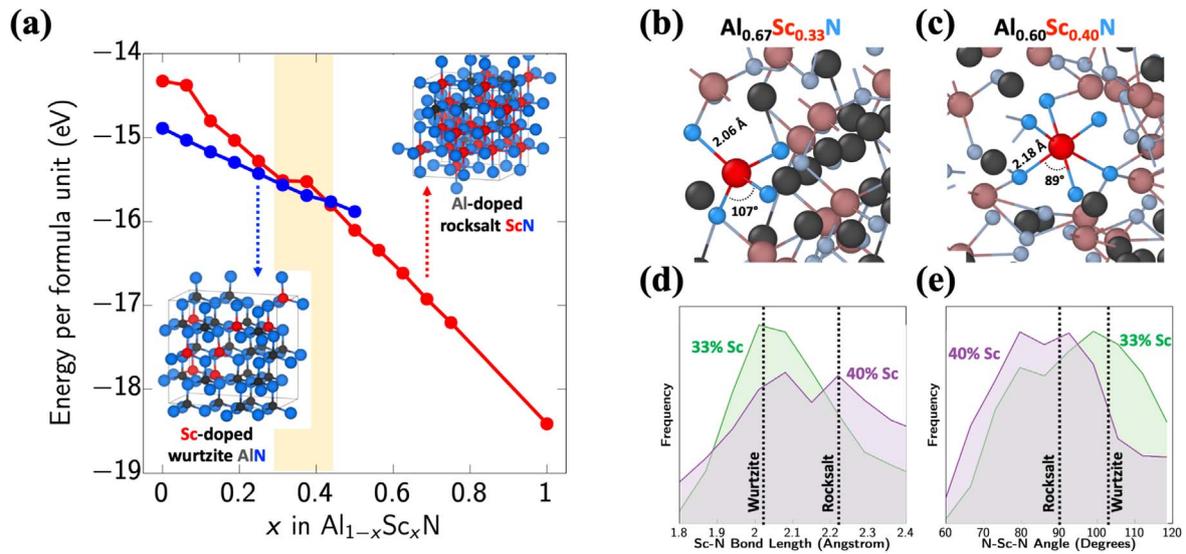
Figure 1. Local structure in $Al_{1-x}Sc_xN$ alloys. (a) Phase boundary and regimes of stability for $Al_{1-x}Sc_xN$ wurtzite and rocksalt structures computed by DFT. These phase boundaries are also supported by the observed local atomic structure around a representative Sc ion in computationally synthesized systems with (b) 33% and (c) 40% Sc content, which are wurtzite-like and rocksalt-like respectively. This difference in local structure is also apparent in the comparisons of (d) Sc–N bond lengths (e) and N–Sc–N bond angles.

Sc-doping for $x < 0.28$ and a rocksalt structure with Sc–N octahedra for $x > 0.43$. In the range $0.28 < x < 0.43$, the wurtzite and rocksalt structures lie within 42.4 meV/atom of each other, which is within the thermal energy at common material synthesis conditions ($k_BT = 86$ meV at 1000 K). This phase boundary is consistent with experimental synthesis by reactive sputtering and observation of phase separation at higher Sc concentrations upon doping [25, 34].

Computational synthesis simulations of a melt-quench schedule were performed that are representative of experimental synthesis of $Al_{1-x}Sc_xN$ using reactive sputtering and pulsed laser deposition. Figures 1(b) and (c) show the local structure around Sc ions in $Al_{0.67}Sc_{0.33}N$ and $Al_{0.6}Sc_{0.4}N$ samples. Highlighted Sc and N atoms depict the tetrahedral (T_h) and octahedral (O_c) coordination present in the systems respectively. The differences between these structures can also be quantified through the Sc–N bond length and the N–Sc–N bond angles. The O_c structure shows a 0.12Å longer bond length compared to T_h structure and the N–Sc–N covalent bond angles are tetrahedral (109°) in the T_h phase but closer to 90° for the octahedral coordination in the rocksalt phase. Figures 1(c) and (d) shows the normalized distribution of bond lengths and bond angles in the 33% and 40% Sc-doped systems. Signatures of both wurtzite and rocksalt structures in the computed bond-length and bond-angle distributions at all compositions, it is noticeable that the wurtzite structure dominates over the rocksalt structure at $x = 0.33$, whereas the rocksalt is more apparent at $x = 0.40$. Isovalent substitutional doping by Sc also results in a reduction in the bandgap of AlN. Sc-doping also results in a softer crystal structure with weaker covalent bonds which improves its piezoelectricity [19] (see SI table S1).

Guided by computational synthesis simulations, we construct these up- and down-polarized ferroelectric $Al_{1-x}Sc_xN$ crystals by substitutionally doping Sc into up and down-

polarized AlN crystals and relaxing the atomic positions within the given cell size.

3.2. Mechanism and kinetics of ferroelectric switching at low applied electric fields

We perform DFT based solid-state NEB simulations of the switching process between the up and down-polarized structures of 25% Sc-doped AlN crystals to identify mechanistic details about the switching process including transition states and energy barriers. Ferroelectric switching occurs along the minimum energy pathway for polarization reversal identified by NEB simulations in the limit of low applied electric where energy barriers are much larger than thermal fluctuations [1]. Figure 2(a) shows the computed PES for the lowest-energy ferroelectric switching pathway in a $Al_{1-x}Sc_xN$ alloy with an energy barrier of 25 meV/atom. This is comparable with the experimental observations of low-field ferroelectric switching in $Al_{0.57}Sc_{0.43}N$ which occurs at 1.9 MV cm^{-1} resulting in a ΔP of 160 μC cm^{-2}, which corresponds to an energy barrier 22 meV/atom [25]. The similarity between experimental switching barriers and the computed NEB barriers suggests that experimental switching occurs along the pathway identified by the NEB simulations.

Intermediate configurations in the NEB snapshots provide atomistic insights into the ferroelectric switching process. Specifically, NEB reveals a highly heterogeneous column-by-column switching mechanism, with nucleation and growth of flipped domains atomic configurations in intermediate NEB images depict partially switched configurations with an unit-cell-wide 180° lateral domain wall between domains with up and down polarization states which is consistent with other first-principles Hamiltonian based calculations and multiscale simulations for the width of 180° domain walls in BTO and defect-free PTO on the order of 5 Å or under two lattice constants [35–37].
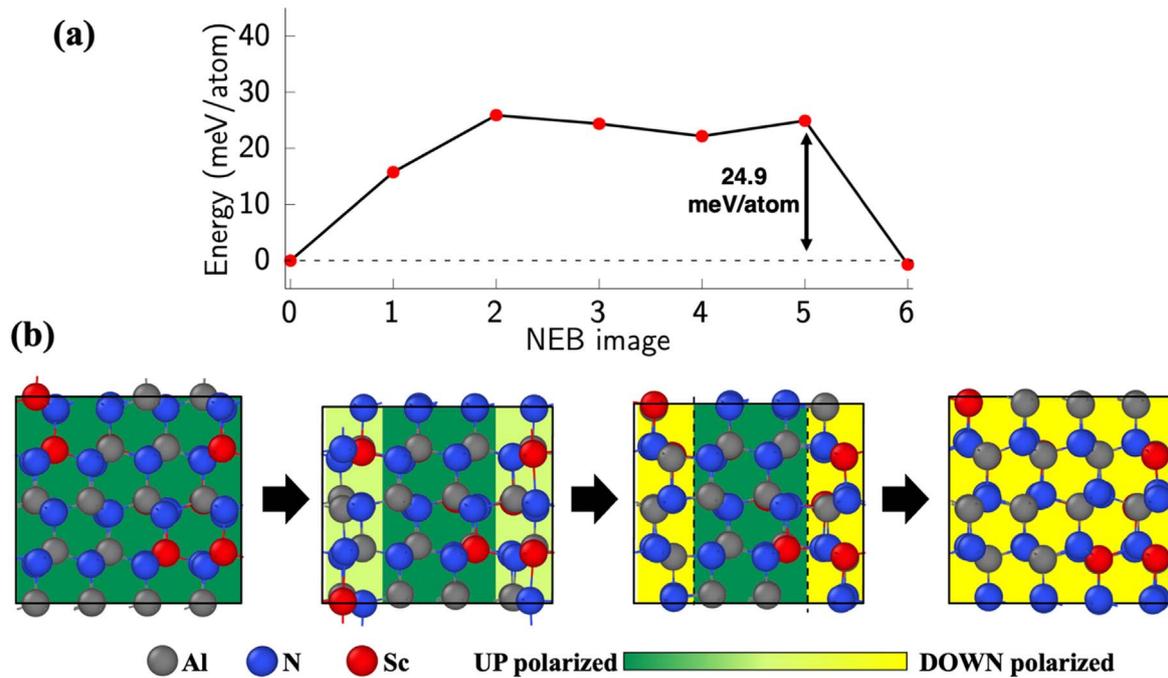
Figure 2. Polarization reversal in zero-field limit. NEB-computed lowest-energy pathway for ferroelectric switching in $Al_{0.75}Sc_{0.25}N$ in the limit of zero applied field (a) contains an energy barrier of 24.9 meV/atom and (b) proceeds via a column-by-column nucleation and growth mechanism.

Even in the absence of extrinsic point defects (like vacancies or anti-site defects), polarization switching in $Al_{1-x}Sc_xN$ alloys is not homogeneous and proceeds through a nucleation and growth process, where columns of Al(Sc)–N–Al(Sc)–N atoms along the field direction undergo polarization switching followed by the lateral growth of this switched domain to encompass the simulation cell. Switching in $Al_{1-x}Sc_xN$ columns is analogous to chain instability in perovskite ferroelectrics, where chains of B-site cations and oxygen anions undergo polarization switching along the field direction before the lateral motion of domain walls along a lateral direction to the applied field [38]. Macroscopic polarization reversal in defect-free $Al_{1-x}Sc_xN$ can be characterized by the KAI model of solid-state phase transformation that involves random and statistically-independent nucleation and growth of reverse domains [39–41] and whose kinetics in these systems is dominated by two-dimensional lateral motion of domain walls, per Ishibashi and Takagi [30, 42]. Such polarization reversal kinetics was recently confirmed by ultrafast x-ray imaging [43] and piezoelectric force microscopy [44] studies of large-size thin-film ferroelectric materials. However, in contrast to traditional perovskite ferroelectrics, where 180° polarization switching occurs through nucleation and growth of 90° domain walls [45], in an uniaxial ferroelectric like $Al_{1-x}Sc_xN$, the domains are separated by only an atomically sharp 180° domain wall. The NEB simulations also show that the saddle point in the pathway exists at the point of nucleation of the polarization-reversed domain. This is consistent with previous molecular dynamics simulations which show that the growth of critical nuclei possesses activation barriers much smaller (20%–50%) than for nucleation [37] (see figure S2).

Unlike the case of GeTe, or other nanoconfined ferroelectric materials and ultrathin ferroelectric films, which undergo homogeneous switching with low activation barriers [30, 46], Sc-doping in AlN biases the PES of the switching process towards a domain formation and growth mechanism.

Inhomogeneous transformation is not-surprising because the barriers for homogeneous transformation for AlN and $Al_{1-x}Sc_xN$ are significantly higher at 256 meV/atom and 453 meV/atom respectively (see figure S3), and proceeds via boron-nitride-like $P6_3/mmc$, the closest centrosymmetric configuration. This difference between nucleation-growth and homogeneous switching barriers is similar to that observed in traditional perovskite ferroelectrics like $BiFeO_3$, where, broadly, the homogeneous switching has a significantly larger barrier than that for nucleation with domain growth driven switching [31].

To understand the effect of piezoelectric volume expansion of AlScN during polarization switching, we also perform NEB simulations of the ferroelectric switching process at fixed volume and cell shape. These constrained NEB simulations reveal a column-by-column nucleation is similar to that in SS-NEB simulations, but with an energy barrier that is 35% larger, indicating that lattice distortion is important in determining the potential energy landscape and activation energy barriers of ferroelectric switching (figure S3).

3.3. Polarization reversal mechanism in field-driven switching at high electric fields

The NEB pathway describes the lowest-energy mechanism of polarization reversal in the absence of an external field. To understand if polarization reversal mechanisms are different for
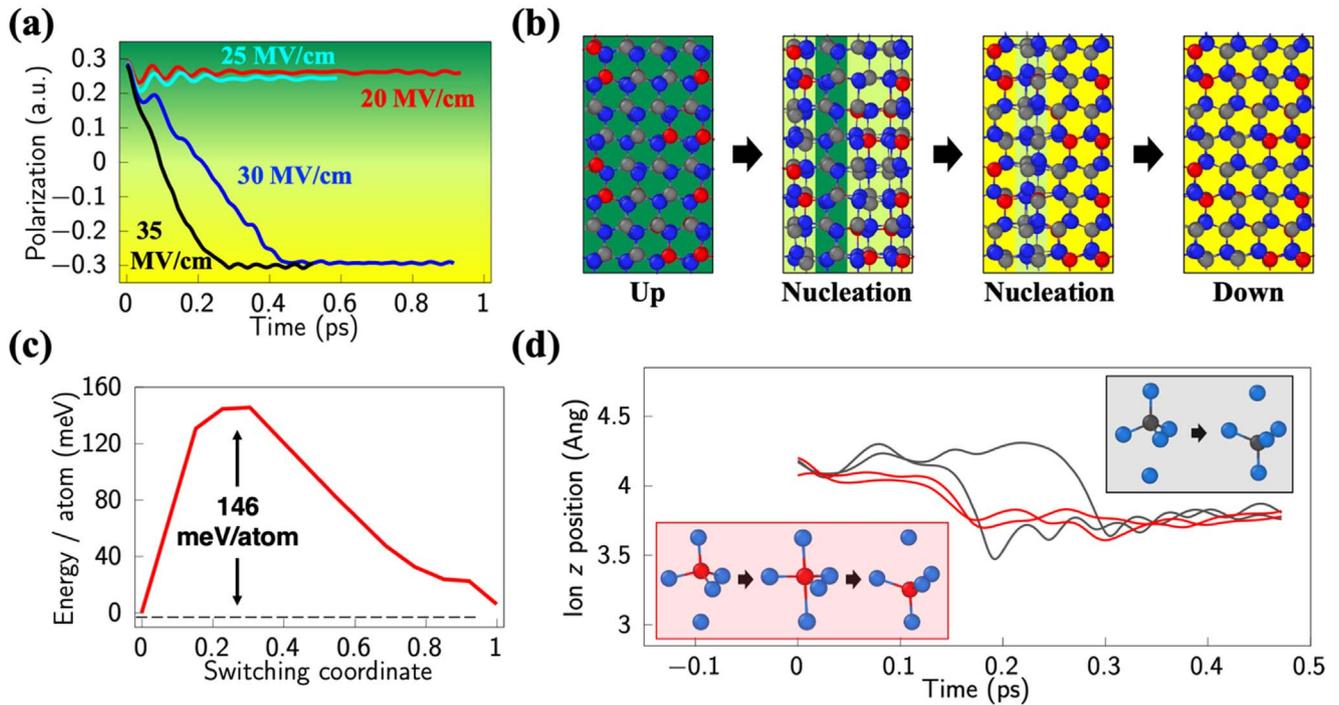
Figure 3. Mechanism of field-driven phase switching. (a) Coercive fields $\geqslant 25$ MV cm^{-1} are necessary to induce switching within 1 ps in Al$_{0.75}$Sc$_{0.25}$N. (b) The field-driven switching mechanism and intermediate structures reflect a nucleation-limited-switching mechanism with independent and simultaneous nucleation of multiple flipped columns. (c) The different mechanism is also reflected in the energy barrier encountered for the switching process, which is approximately 6 times larger than that predicted by NEB for a single nucleation event (d) Plot of Sc and Al ionic positions during the polarization reversal process shows that Sc ions (red) begin to switch first and more gradually relative to the surrounding Al ions (gray). The insets reveal the difference in pathway for switching of Al and Sc ion, including the metastable five-fold coordinated h-ScN structure.

field-driven switching, we also performed quantum MD simulation in the presence of externally-applied electric fields. Figure 3(a) shows the computed polarization of the Al$_{0.75}$Sc$_{0.25}$N crystal as a function of time during the MD simulation at four different applied fields of 20, 25, 30, and 35 MV cm^{-1}.

The simulation cell remains in the up-polarized state (i.e. does not undergo ferroelectric switching within 1 ps) for externally-applied fields of 20 and 25 MV cm^{-1}. These applied fields are significantly larger than the experimental coercive of 4 MV cm^{-1} [25]. The large magnitude of the applied field required to induce polarization reversal is partly attributed to the necessity of inducing ferroelectric switching within the timescale of ~1 ps accessible by *ab initio* MD simulations and partly to the fact that real ferroelectrics switch because switching between polarized domains is often mediated by nanoscale defects both in the bulk and at surfaces [47], which play a governing role on ferroelectric domain nucleation [48–50]. Such surface defects and lattice termination effects are not present in periodic supercells used in *ab initio* simulations. Larger applied electric fields of 30 and 35 MV cm^{-1} induce polarization switching from a value of 0.3 to −0.3 au, with the larger electric-field resulting in faster phase switching.

The Al$_{0.75}$Sc$_{0.25}$N system undergoes ultrafast sub-ps polarization switching beyond a critical field value of 30 MV cm^{-1} consistent with predicted ferroelectric switching times [51–53] for both homogeneous switching and domain wall mediated switching in materials like La:BiFeO$_3$. This

rapid kinetics is extremely promising because a pathway to sub-ns switching is a key milestone for device applications [51, 54]. Specifically, polarization reversal in 0.3–0.4 ps is consistent with the time taken for the propagation of sound (6000 m s^{-1} [55]) through the 20 Å Al$_{0.75}$Sc$_{0.25}$N crystal.

Figure 3(b) shows the intermediate atomic configurations in an electric-field-driven ferroelectric switching pathway. In contrast to the column-by-column nucleation-and-growth mechanism observed in NEB simulations, switching under the influence of these high electric fields proceeds through a nucleation-limited-switching pathway [31] where all the Sc regions in the supercell independently and simultaneously undergo switching with limited propagation of flipped domains. This behavior is consistent with observations in ferroelectric Pb(Zr,Ti)O$_3$ [56] and BiFeO$_3$ [57] and other polycrystalline thin films [58] which also demonstrate this alternate inhomogeneous switching mechanism at large coercive fields and is consistent with a recent phase-field study that hypothesizes a nucleation-limited mechanism for ultrafast switching [59]. Direct field-driven polarization reversal pathway is accompanied by a larger energy barrier (146 meV/atom) for phase-switching (figure 3(c)). Figure 3(d) shows the time-profile of the displacement of all cations during the phase transition. Sc ions in Al$_{0.75}$Sc$_{0.25}$N behave differently to Al ions in two respects: (1) the Sc ion undergoes phase switching before the Al ions and (2) the Sc ions undergo a gradual switching process in contrast to Al ions, which undergoes a sudden transition between their up- and down-polarization atomic positions. The insets in figure 3(d) show the intermediate atomic
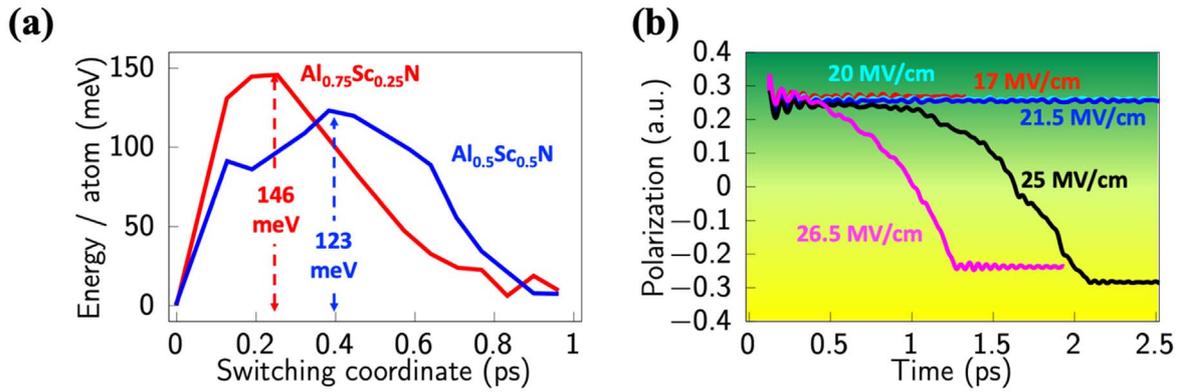
Figure 4. Effect of Sc concentration of polarization reversal. Energy barrier for field-driven phase transformation goes down from 146 meV/atom to 123 meV/atom as the Sc content increases from 25% to 50%. (b) Reduced energy barriers are also reflected in the lower coercive field of 25 MV cm^{-1} for $Al_{0.5}Sc_{0.5}N$.

configurations for the Al and Sc ions during this switching process. It demonstrates that the intermediate h-ScN configuration with P6$_3$/mmc symmetry is significantly more stable that the corresponding h-AlN configuration, which enables Sc ions to undergo gradual switching [60].

The significantly larger barrier for the field-driven polarization switching process is indicative of the existence of multiple, independent nucleation events in the transition state configuration, each occurring with an activation barrier of ~25 meV/atom as seen in figure 2. In this 'nucleation-limited switching' regime, multiple nucleation events are made possible in the presence of strong applied electric fields, which reduce the activation energy barrier for nucleation events by biasing the PES towards flipped configurations [61, 62]. In the absence of externally-applied electric fields, the relatively high energy cost of nucleation events favors a 'nucleation and growth' mechanism, where a single (or few) nucleation events are followed by more energetically feasible growth of flipped domains.

3.4. Effect of Sc concentration and distribution on polarization reversal

Point defects like substitutional Sc dopants can influence the kinetics and thermodynamics of polarization switching in three ways [35]—they can affect the relative stability of the ferroelectric and non-polar states and modify the Curie temperature [63], they can act as nucleation sites for ferroelectric switching and finally, they can act as pinning sites for moving domain walls and transformation fronts [3, 64]. Isovalent dopants like Sc (so-called random bond defects) affect the height of the energy barrier between degenerate polarizations states and the coercive field [47, 48, 65] as seen in perovskite ferroelectrics [51, 66, 67]. This is in contrast to polarized and charged point defects (so-called random field defects), which break the degeneracy of polarization states to favor one orientation over the other. Random-bond defect behavior of Sc sites is evident in the near-degeneracy of the up- and down-polarized structures in NEB simulations (figures 2 and S3).

Figure 4(a) compares the field-driven switching barrier at 30 MV cm^{-1} in two $Al_{1-x}Sc_xN$ alloys—$Al_{0.75}Sc_{0.25}N$ and

$Al_{0.5}Sc_{0.5}N$. The barrier for phase switching decreases from 146 meV/atom for 25% Sc-doping to 123 meV/atom at 50% Sc-doping. This is accompanied by a reduction in the computed coercive field. Fields as low as 25 MV cm^{-1} are sufficient to induce polarization reversal in $Al_{0.5}Sc_{0.5}N$, whereas stronger fields $\geqslant$ 30 MV cm^{-1} are necessary for $Al_{0.75}Sc_{0.25}N$. This is consistent with experimental observations where increasing Sc content in AlScN alloys reduces the coercive field from 4 to 2 MV cm^{-1} [25]. Both the reduced barrier and reduced coercive fields are expected outcomes of an increase in the concentration of random-bond defects. Beyond changes in the PES and the activation barrier for phase switching, the nucleation-limited-switching mechanism of polarization reversal dominates even at higher concentrations of Sc (movie S1).

Polarization reversal in both high-field-driven QMD simulations (figure 3 and movie S1) and low-field NEB pathway (figure 2) is initiated at Sc-rich regions. Local inhomogeneities in the distribution of random bond defects (i.e. Sc ions) in the alloy are necessary to trigger a ferroelectric instability and induce cooperative displacement of atoms leading to polarization switching [38, 68–70]. Figure S4 shows that activation energy barriers for homogeneous switching are an order of magnitude larger (~450 meV/atom) than those computed for inhomogeneous switching in $Al_{1-x}Sc_xN$ alloys. Therefore, this inhomogeneity plays a key role in determining the coercive voltage as well as the net polarization of the system. To demonstrate this, we perform *ab initio* field induced switching simulations on a 25% Sc-doped $Al_{1-x}Sc_xN$ with a highly inhomogeneous distribution of Sc dopants. The inhomogeneous crystal is constructed by segregating all Sc ions to the left half of the simulation cell, such that its local concentration is 50% Sc, whereas the right half of the simulation cell becomes undoped AlN.

Figure 5 shows the observed change in polarization of the inhomogeneously-doped $Al_{0.75}Sc_{0.25}N$ crystal system as a function of time during the field-driven switching QMD simulation. Rapid, but partial, switching occurs in the system at an applied field of 25 MV cm^{-1}, which is smaller than the measure coercive field for $Al_{0.75}Sc_{0.25}N$ with a homogeneous Sc distribution. Figures 5(b)–(e) show snapshots of the switching system at times t = 0, 0.5, 1.5 and 3.5 ps during the
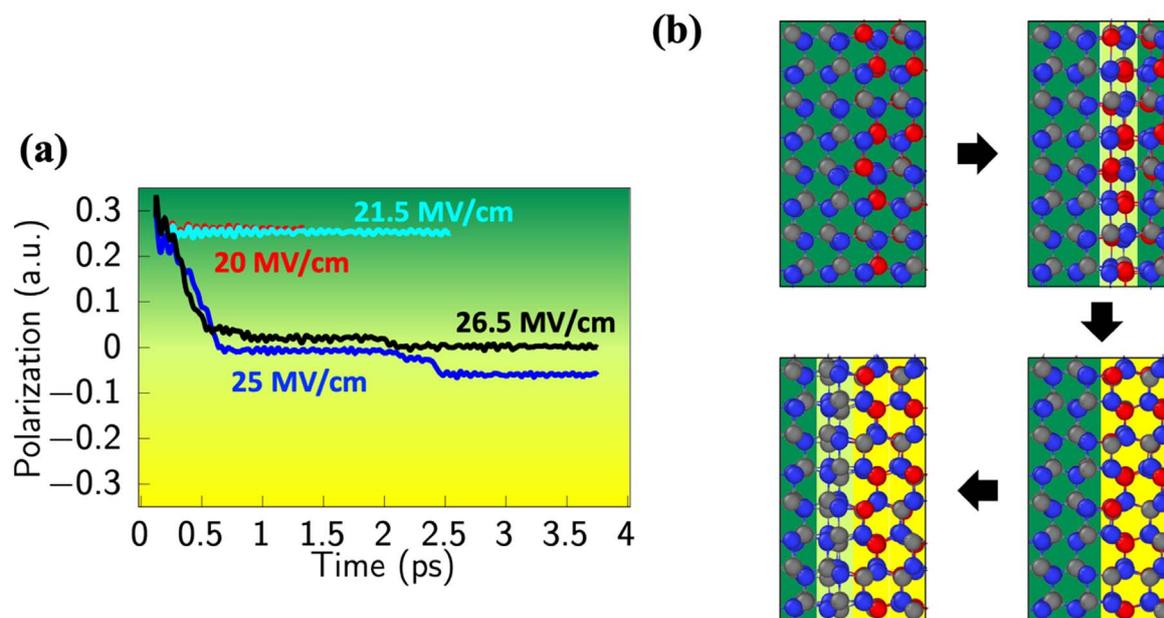
Figure 5. Effect of Sc distribution on polarization reversal. (a) Change in polarization of the inhomogeneous simulation cell as a function of time. (b) Snapshots of important atomic configurations in the switching system. Rapid polarization switching in the Sc-rich half of the simulation cell results in a steady state configuration with a partially-switched boundary between the switched and unswitched domains.

simulation, reflecting important configurations during the switching process. Rapid initial switching occurs during 0–0.7 ps and is limited to polarization switching in the Sc-rich half of the crystal. After this, the system reaches a new partially-switched equilibrium state with half the simulation cell having undergone polarization reversal, since the applied field is greater than the coercive field for the left half of the cell ($Al_{0.5}Sc_{0.5}N$), but lesser than the coercive field for the right half of simulation cell (undoped AlN). Figure 5(e) represents the final steady state of the partially-switched crystal under the application of 25 MV cm^{-1}, containing a partially switched configuration at the boundary between the Sc-rich and Sc-poor domains. The sharp domain wall is identical to theorized atomically sharp domain walls in perovskite ferroelectrics like BTO, which pass through the plane of Ti–O chains.

4. Conclusion

DFT-NEB and electric-field-driven QMD simulations are used to investigate the different mechanisms of ferroelectric switching in two regimes—zero-to-low electric fields and strong applied fields. NEB simulations of the ferroelectric switching in the low-field limit reveal a minimum barrier of 25 meV/atom for the defect-free single crystal, consistent with experimentally computed coercive fields and polarizations. NEB simulations identified a traditional column-by-column nucleation and growth mechanism of the lowest-energy pathway for polarization reversal, whose kinetics and energetics are significantly affected by ferroelastic expansion.

Direct-switching QMD simulations in intense applied fields show polarization reversal along a different nucleation-limited-switching pathway—ferroelectric switching begins at all Sc sites followed by correlated motion of all other Al ions.

Sc ions pass through the metastable five-fold h-ScN configuration possessing zero polarization, along with a strong dependence of domain wall speed on applied field.

Energy barriers for polarization reversal and coercive fields in both regimes were found to depend strongly on Sc concentration with field-driven switching barriers lower by 23 meV/atom at increased Sc concentrations. Further, local inhomogeneities in Sc concentration can greatly affect both the onset and extent of ferroelectric switching with inhomogeneous Sc distribution leading to a reduction both in the activation barrier as well as the coercive field.

Data availability statement

The data that support the findings of this study are available upon reasonable request from the authors.

ORCID iDs

Aravind Krishnamoorthy ⬤ https://orcid.org/0000-0001-6778-2471

References

[1] Morozovska A N *et al* 2008 Local polarization switching in the presence of surface-charged defects: microscopic mechanisms and piezoresponse force spectroscopy observations *Phys. Rev.* B **78** 054101

[2] Guan X X *et al* 2020 Unconventional ferroelectric switching via local domain wall motion in multiferroic epsilon-Fe$_2$O$_3$ films *Adv. Electron. Mater.* **6** 1901134

[3] Li X Y *et al* 2018 Domain wall motion in perovskite ferroelectrics studied by the nudged elastic band method *J. Phys. Chem.* C **122** 3091–100

[4] Seidel J 2015 Ferroelectric nanostructures domain walls in motion *Nat. Nanotechnol.* **10** 109–10

[5] Jablonski M L *et al* 2016 Asymmetric response of ferroelastic domain-wall motion under applied bias *ACS Appl. Mater. Interfaces* **8** 2935–41

[6] Scott J F 2000 *Ferroelectric Memories* (*Advanced Microelectronics*) (Berlin: Springer) xvi p 248

[7] Contreras J R *et al* 2003 Resistive switching in metal-ferroelectric-metal junctions *Appl. Phys. Lett.* **83** 4595–7

[8] Cho Y 2007 Nanoscale ferroelectric information storage based on scanning nonlinear dielectric microscopy *J. Nanosci. Nanotechnol.* **7** 105–16

[9] Wu M H and Zeng X C 2016 Intrinsic ferroelasticity and/or multiferroicity in two-dimensional phosphorene and phosphorene analogues *Nano Lett.* **16** 3236–41

[10] Zhang S J *et al* 2005 Piezoelectric materials for high power, high temperature applications *Mater. Lett.* **59** 3471–5

[11] Muralt P, Polcawich R G and Trolier-McKinstry S 2009 Piezoelectric Thin films for sensors, actuators, and energy harvesting *MRS Bull.* **34** 658–64

[12] Materano M *et al* 2020 Polarization switching in thin doped HfO$_2$ ferroelectric layers *Appl. Phys. Lett.* **117** 262904

[13] Xu X *et al* 2021 Kinetically stabilized ferroelectricity in bulk single-crystalline HfO$_2$:Y *Nat. Mater.* **20** 826–32

[14] Nukala P *et al* 2021 Reversible oxygen migration and phase transitions in hafnia-based ferroelectric devices *Science* **372** 630

[15] Wang P *et al* 2021 Fully epitaxial ferroelectric ScAlN grown by molecular beam epitaxy *Appl. Phys. Lett.* **118** 223504

[16] Hayden J *et al* 2021 Ferroelectricity in boron-substituted aluminum nitride thin films *Phys. Rev. Mater.* **5** 044412

[17] Sarmiento-Pérez R *et al* 2015 Prediction of stable nitride perovskites *Chem. Mater.* **27** 5957–63

[18] Chen P-Y *et al* 2021 Hafnium oxide-based ferroelectric devices for computing-in-memory applications *Phys. Status Solidi* a **218** 2000635

[19] Jena D *et al* 2019 The new nitrides: layered, ferroelectric, magnetic, metallic and superconducting nitrides to boost the GaN photonics and electronics eco-system *Japan. J. Appl. Phys.* **58** SC0801

[20] Mikolajick T *et al* 2021 Next generation ferroelectric materials for semiconductor process integration and their applications *J. Appl. Phys.* **129** 100901

[21] Bernardini F, Fiorentini V and Vanderbilt D 1997 Spontaneous polarization and piezoelectric constants of III-V nitrides *Phys. Rev.* B **56** 10024–7

[22] Biswas B and Saha B 2019 Development of semiconducting ScN *Phys. Rev. Mater.* **3** 020301

[23] Akiyama M, Kano K and Teshigahara A 2009 Influence of growth temperature and scandium concentration on piezoelectric response of scandium aluminum nitride alloy thin films *Appl. Phys. Lett.* **95** 162107

[24] Akiyama M *et al* 2009 Enhancement of piezoelectric response in scandium aluminum nitride alloy thin films prepared by dual reactive cosputtering *Adv. Mater.* **21** 593

[25] Fichtner S *et al* 2019 AlScN: a III–V semiconductor based ferroelectric *J. Appl. Phys.* **125** 114103

[26] Wang J *et al* 2020 A film bulk acoustic resonator based on ferroelectric aluminum scandium nitride films *J. Microelectromech. Syst.* **29** 741–7

[27] Yamamoto N, Yagi K and Honjo G 1980 Electron-microscopic studies of ferroelectric and ferroelastic Gd$_2$(Moo$_4$)$_3$: IV. Polarization reversal and field-induced phase-transformation *Phys. Status Solidi* a **62** 657–64

[28] Snoeck E *et al* 1994 Electron-microscopy study of ferroelastic and ferroelectric domain-wall motions induced by the *in situ* application of an electric-field in BaTiO$_3$ *Phase Transit.* **46** 77–88

[29] Tan X L and Shang J K 2002 *In situ* transmission electron microscopy study of electric-field-induced grain-boundary cracking in lead zirconate titanate *Phil. Mag.* A **82** 1463–78

[30] Liu S, Grinberg I and Rappe A M 2016 Intrinsic ferroelectric switching from first principles *Nature* **534** 360

[31] Xu B *et al* 2017 Intrinsic polarization switching mechanisms in BiFeO$_3$ *Phys. Rev.* B **95** 104104

[32] Rosen J *et al* 2007 Amorphous and crystalline phases in thermal quench simulations of alumina *J. Chem. Phys.* **126** 204709

[33] Umari P and Pasquarello A 2002 *Ab initio* molecular dynamics in a finite homogeneous electric field *Phys. Rev. Lett.* **89** 157602

[34] Hoglund C *et al* 2010 Wurtzite structure Sc$_{1-x}$Al$_x$N solid solution films grown by reactive magnetron sputter epitaxy: structural characterization and first-principles calculations *J. Appl. Phys.* **107** 123515

[35] Pramanick A *et al* 2012 Domains, domain walls and defects in perovskite ferroelectric oxides: a review of present understanding and recent contributions *Crit. Rev. Solid State Mater. Sci.* **37** 243–75

[36] Padilla J, Zhong W and Vanderbilt D 1996 First-principles investigation of 180 degrees domain walls in BaTiO$_3$ *Phys. Rev.* B **53** R5969–73

[37] Shin Y H *et al* 2007 Nucleation and growth mechanism of ferroelectric domain-wall motion *Nature* **449** 881–U7

[38] Lichtensteiger C *et al* 2012 Ferroelectricity in ultrathin-film capacitors *Oxide Ultrathin Films* (New York: Wiley) 265–230

[39] Li J *et al* 2004 Ultrafast polarization switching in thin-film ferroelectrics *Appl. Phys. Lett.* **84** 1174–6

[40] Merz W J 1956 Switching time in ferroelectric BaTiO$_3$ and its dependence on crystal thickness *J. Appl. Phys.* **27** 938–43

[41] Merz W J 1954 Domain formation and domain wall motions in ferroelectric BaTiO$_3$ single crystals *Phys. Rev.* **95** 690–8

[42] Ishibashi Y and Takagi Y 1971 Note on ferroelectric domain switching *J. Phys. Soc. Japan* **31** 506–10

[43] Grigoriev A *et al* 2006 Nanosecond domain wall dynamics in ferroelectric Pb(Zr, Ti)O$_3$ thin films *Phys. Rev. Lett.* **96** 187601

[44] Gruverman A *et al* 2005 Direct studies of domain switching dynamics in thin film ferroelectric capacitors *Appl. Phys. Lett.* **87** 082902

[45] Lente M H *et al* 2004 90 degrees domain wall relaxation and frequency dependence of the coercive field in the ferroelectric switching process *J. Appl. Phys.* **95** 2646–53

[46] Kolobov A V *et al* 2014 Ferroelectric switching in epitaxial GeTe films *APL Mater.* **2** 066101

[47] Gao P *et al* 2011 Revealing the role of defects in ferroelectric switching with atomic resolution *Nat. Commun.* **2** 591

[48] Jesse S *et al* 2008 Direct imaging of the spatial and energy distribution of nucleation centres in ferroelectric materials *Nat. Mater.* **7** 209–15

[49] Landauer R 1957 Electrostatic considerations in batio3 domain formation during polarization reversal *J. Appl. Phys.* **28** 227–34

[50] Miller R C and Weinreich G 1960 Mechanism for the sidewise motion of 180-degrees domain walls in barium titanate *Phys. Rev.* **117** 1460–6

[51] Parsonnet E *et al* 2020 Toward intrinsic ferroelectric switching in multiferroic BiFeO$_3$ *Phys. Rev. Lett.* **125** 067601

[52] Chang H J *et al* 2011 Watching domains grow: *in situ* studies of polarization switching by combined scanning probe and scanning transmission electron microscopy *J. Appl. Phys.* **110** 052014

[53] Chang S C *et al* 2018 Physical origin of transient negative capacitance in a ferroelectric capacitor *Phys. Rev. Appl.* **9** 014010

[54] Alessandri C *et al* 2018 Switching dynamics of ferroelectric Zr-Doped HfO$_2$ *IEEE Electron Device Lett.* **39** 1780–3

[55] Tsubouchi K and Mikoshiba N 1985 Zero-temperature-coefficient SAW Devices on AlN epitaxial films *IEEE Trans. Sonics Ultrason.* **32** 634–44

[56] Lohse O *et al* 2001 Relaxation mechanism of ferroelectric switching in Pb(Zr,Ti)O-3 thin films *J. Appl. Phys.* **89** 2332–6

[57] Boyn S *et al* 2017 Learning through ferroelectric domain dynamics in solid-state synapses *Nat. Commun.* **8** 14736

[58] Kim T H *et al* 2011 Polarity-dependent kinetics of ferroelectric switching in epitaxial BiFeO$_3$(111) capacitors *Appl. Phys. Lett.* **99** 012905

[59] Yang T *et al* 2020 Domain dynamics under ultrafast electric-field pulses *Phys. Rev. Lett.* **124** 107601

[60] Farrer N and Bellaiche L 2002 Properties of hexagonal ScN versus wurtzite GaN and InN *Phys. Rev.* B **66** 201203

[61] Emelyanov A Y 2005 Coherent ferroelectric switching by atomic force microscopy *Phys. Rev.* B **71** 132102

[62] Morozovska A N *et al* 2007 Piezoresponse force spectroscopy of ferroelectric-semiconductor materials *J. Appl. Phys.* **102** 114108

[63] Alpay S P *et al* 2004 Can interface dislocations degrade ferroelectric properties? *Appl. Phys. Lett.* **85** 2044–6

[64] Yang S M *et al* 2012 Nanoscale observation of time-dependent domain wall pinning as the origin of polarization fatigue *Adv. Funct. Mater.* **22** 2310–7

[65] Nattermann T, Shapir Y and Vilfan I 1990 Interface pinning and dynamics in random-systems *Phys. Rev.* B **42** 8577–86

[66] Zhang L *et al* 2019 Enhanced pyroelectric properties of Bi$_{1-x}$La$_x$FeO$_3$ thin films *APL Mater.* **7** 111111

[67] Prasad B *et al* 2020 Ultralow Voltage manipulation of ferromagnetism *Adv. Mater.* **32** 2001943

[68] Geneste G, Bousquet E and Ghosez P 2008 New insight into the concept of ferroelectric correlation volume *J. Comput. Theor. Nanosci.* **5** 517–20

[69] Zhao D *et al* 2019 Depolarization of multidomain ferroelectric materials *Nat. Commun.* **10** 2547

[70] Scott J F 2010 Switching of ferroelectrics without domains *Adv. Mater.* **22** 5315–7